V European Conference on Computational Fluid Dynamics
ECCOMAS CFD 2010
J. C. F. Pereira and A. Sequeira (Eds)
Lisbon, Portugal, 14–17 June 2010

NUMERICAL SIMULATION OF A MARINE PROPELLER IN A CROSS FLOW

Seth D. Schroeder[*], Charles M. Dai[†]

[*]Naval Surface Warfare Center, Carderock Division
West Bethesda, Maryland, USA
e-mail: seth.schroeder@navy.mil

[†]Naval Surface Warfare Center, Carderock Division
West Bethesda, Maryland, USA
e-mail: charles.dai@navy.mil

Key words: marine, propeller, RANS, unsteady, cross flow

Abstract. *A propeller in an inclined shaft arrangement has been simulated using a Reynolds-Averaged Navier-Stokes (RANS) solver. The RANS solver simulates a propeller subjected to a cross flow similar to that experienced during ship maneuvering. The simulations were performed with increasing complexity to gain confidence in the solution process. Initial steady-state cases involved uniform inflow conditions which could be compared to experimental data. The simulations then grew in complexity to consist of time accurate solutions in which the propeller was subjected to a cross flow component of velocity. Cross flow components of velocity in opposite directions were examined to represent a ship maneuvering in either direction relative to the rotation of the propeller. This paper describes in detail the full process used for the simulations. Meshing techniques, solver settings, and post processing quantities are all examined. Comparisons are made between the experimental open water thrust and torque data of propeller P4990 with the computational results. The RANS solver was further used to predict the hydrodynamic performance of P4990 subjected to a cross flow. The effect of the propeller trialing wake on the downstream rudder is discussed. The magnitude of propeller side forces generated was shown to be significant for a cross flow angle of 23 degrees. These simulations have demonstrated existing propeller modeling capabilities and further developed capabilities towards the modeling of a ship performing a maneuver.*

1 INTRODUCTION

Marine propellers consist of complex geometry involving advanced airfoil sections which are operating in a non-uniform velocity field at the stern region of a ship. Historically, naval architects have relied on numerical tools such as panel and vortex lattice codes for design and analysis. These tools have been extensively developed to provide sufficient accuracy for the prediction of powering performance during the design process[1]. However, the predictive capability for propeller performance in a cross flow due to a ship maneuver requires improvement due to the uncertainty in propeller trailing edge wake modeling and the inability of potential flow based methods in modeling viscous effects.

Ship maneuvering is a complex problem because the propeller experiences inflow velocities that vary significantly from design conditions. It is necessary to predict the forces generated by the propeller when subjected to these velocities in order to successfully model an entire ship system in a prescribed maneuver.

Computational methods solving the Reynolds-averaged Navier-Stokes (RANS) equations have proved to be successful at predicting the performance of marine propellers[2]. This study will examine the use of RANS for an off design propeller simulation of interest by introducing a cross flow velocity component to the case. The prescribed angle of the cross flows are representative of the velocities an operational propeller would experience during an actual ship maneuver[3]. The propeller is also realistically modeled using an inclined shaft arrangement similar to an actual application. In addition to the transverse component of velocity due to the cross flow, the inclined shaft adds a downward component of velocity relative to the propeller axis of rotation.

The trailing wake of the propeller will also be examined for the effects it would have on a notional rudder. This interaction has been studied extensively in the hydrodynamics field[4] as it is of importance to the design of several ship systems.

The objective of this study is to numerically examine the effects of a ship maneuver on propeller performance, and to study the downstream wake characteristics caused by a propeller during this maneuver.

2 ANALYSIS

The analysis of this study began with domain and mesh generation. All of the meshing was completed using the commercially available Ansys' ICEM CFD. After meshing was completed, the simulations were completed using Ansys' Fluent. The first solutions completed were steady flow cases to serve as a baseline comparison with existing experimental data. This initial simulation was completed to gain confidence in the solution process. To gain further confidence, a mesh-dependency study was completed with the steady flow cases. Because these initial cases were steady with a uniform inflow, the flow field was periodic across each blade and the simulation could be simplified by using a separate single blade passage mesh. The unsteady flow cases then began with a straight flight (no cross flow) simulation including an inclined shaft arrangement to compare with experimental data. These initial unsteady cases could not take advantage of periodicity because of the inclined shaft arrangement. Finally, cases were studied with cross flow components of velocity.

2.1 Domain and Meshing

The propeller of interest was propeller P4990. It is a 5-bladed propeller with a model scale diameter of 15.856 inches. The configuration for computations included an upstream shaft of diameter 0.3*D, where D is the diameter of the propeller. The computational domain was sized such that the inlet and outlet boundaries were 2*D upstream and downstream from the propeller blade. The domain extended 1*D from the tip of the blade in the radial direction. These distances were assumed to be adequate based on conclusions of previous studies [2]. The geometry for the blade, hub, and shaft were generated using NURBS surface definition codes and converted to a three-dimensional IGES file. An illustration of the generated domain is seen in Figure 1.

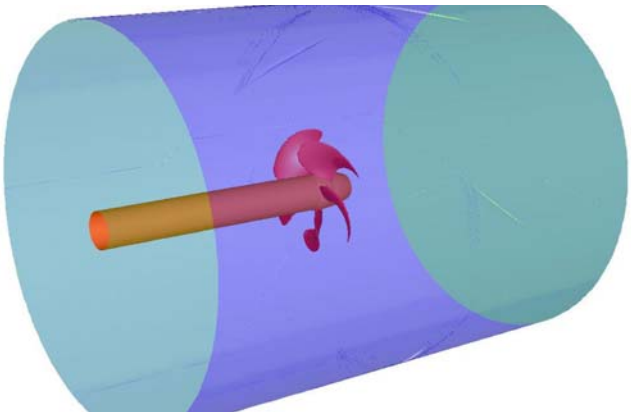

Figure 1 - An illustration of the generated domain.

A structured hexahedral scheme was used to avoid excessive diffusion in the flow field [5]. The type of blocking used was generally H-O type topology. An O-grid was used around the root of the blade, and modified with a Y-block at the leading and trailing edges to give a better definition between the pressure and suction side of the blade. This topology has been validated for several sets of propeller and waterjet performance data[7]. An overhead example illustration of this O-grid topology modified with Y-blocks is seen in Figure 2. This figure is representative of the topology used but is not of the exact geometry. Because of the curvature at the tip of the blade, an O-grid was used on the surface to improve cell quality. An illustration of the O-grid on the blade surface is seen in Figure 3.

Figure 2 - An illustration of O-grid topology modified with Y-blocks at the leading and trailing edges of the blade.

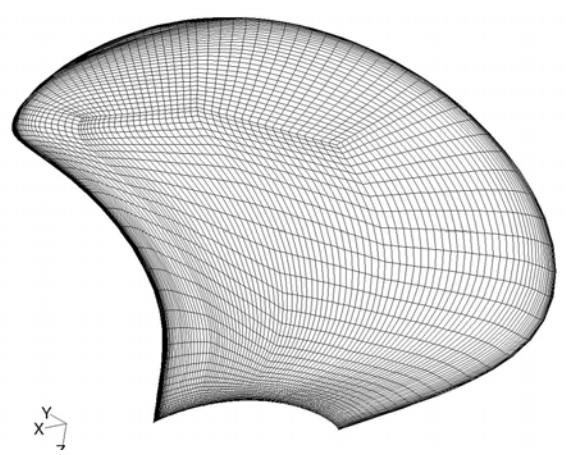

Figure 3 - An illustration of O-grid type mesh on the blade surface.

The mesh sizes were designed to leverage wall functions to decrease the number of cells and computing time. This allowed the cell spacing at the wall to be set such that the wall y+ values ranged from approximately 25 to 80. Wall y+ is defined as:

$$y^+ = \frac{\rho u_\tau y}{\mu} \tag{1}$$

where y = distance to the wall, u_τ = friction velocity, ρ = density, and μ = dynamic viscosity. This first cell spacing off the wall was used on all wall boundaries which included the blades, shaft, and hub. After the first cell from the wall, the spacing was constrained by a geometric growth rate of 1.1 – 1.2. This growth rate defines how large each cell can be as distance from the wall increases. For example, if a growth rate of 1.1 is used, the second cell layer is 10% larger than the first cell layer. The growth rate is used until the cell thickness reaches the prescribed maximum thickness at which point a constant spacing is used.

The mesh was manually refined to meet two primary quality criteria: the minimum cell angle and the 2x2x2 determinant. The minimum cell angle is determined by the smallest internal angle of an element. An angle of 90° indicates a perfectly cubic element and an angle of 0° indicates a degenerate element. The 2x2x2 determinant is a measure of the skewness of the cell and it is defined as the ratio of the smallest determinant of the Jacobian matrix divided by the largest determinant of the Jacobian matrix. A 2x2x2 determinant of 1 indicates a perfectly regular element. A determinant of 0 or less indicates and element which has a degenerate edge or is inverted. Because mesh quality impacts solution stability and accuracy, the minimum internal angle was to be above 18° and the smallest 2x2x2 determinant was to be above 0.4. The mesh was manually refined until both of these conditions were satisfied.

Several unique meshes were generated for this study using the above outlined procedure. The final set of meshes included a single blade passage mesh which takes advantage of periodicity, a refined single blade passage mesh to give confidence in mesh independence, and a full propeller mesh for unsteady cross flow cases in which the domain is not periodic. A summary of the final mesh sizing is seen in Table 1.

Mesh Description	Mesh Size (cells)
Single blade passage	1 million
Refined single blade passage	2 million
Full 5-bladed propeller	5 million

Table 1 - Generated mesh sizing and descriptions

2.2 Solution Strategies

The inlet of the domain was prescribed as a velocity-inlet boundary condition. Fluent uses the specified velocity vector to calculate a mass flow into the domain and the corresponding momentum flux through the boundary. The inlet velocity vector was varied to simulate an inclined shaft arrangement and/or cross flow components as opposed to changing the grid orientation. The outlet of the domain was prescribed as a pressure-outlet boundary condition. At this boundary a static pressure is specified which is set equal to the reference pressure of the domain. The far-field boundaries were set to free-stream conditions such that they did not alter the flow when a non-axial inlet velocity was specified.

The k-ε turbulence model was used for all of the simulations in the study[8]. The k-ε turbulence model is designed to take advantage of wall $y+$ values above 30 and wall functions. As previously stated, the wall $y+$ values designed into the mesh ranged from 25 to 80 to allow for the use of wall functions. Fluent uses a two-layer wall function model which subdivides the whole domain into a viscosity-affected region and a fully-turbulent region.

The initial solution was started with low under-relaxation factors set for all parameters. This corresponds to an extremely damped system which is very stable during the beginning iterations. As a realistic solution began to emerge, the under-relaxation factors were raised to allow for faster convergence. Convergence was established through the standard drop in residuals and also by monitoring the blade forces and average quantities such as pressure on the blade surfaces.

3 RESULTS

The main identifier of a marine propeller operating condition is the advance coefficient, J_a. Advance coefficient is defined as:

$$J_a = \frac{V_S}{nD} \tag{2}$$

where V_S = ship speed (domain inlet velocity), n = rotations per second of the propeller, and D = propeller diameter. Given the previously defined model scale diameter, the inlet velocities were set such that the Reynolds number for the simulations was on the order of 1-2 million based on the chord length at $0.7R$, where R is the propeller radius. This Reynolds number corresponds to typical model scale experiments with inflow velocities on the order of 10-30 ft/s, such as the data set used for comparison later in the study. The advance coefficient was varied to achieve a range of operating conditions for the different simulations.

The main global quantities used for comparison with experimental results as well as comparison between simulations are thrust, torque, and efficiency. These quantities are converted to non-dimensional parameters to allow consistent comparison. These variables are defined as:

$$K_T = \frac{Thrust}{\rho n^2 D^4} \tag{3}$$

$$K_Q = \frac{Torque}{\rho n^2 D^5} \tag{4}$$

$$\eta = \frac{J_a K_T}{2\pi K_Q} \tag{5}$$

where K_T = thrust coefficient, K_Q = torque coefficient, and η = open water efficiency. The force values of thrust and torque are computed by integrating the forces on the blade surfaces and do not include the shaft or the hub. When these three quantities are plotted with a range of advance coefficients as the independent variable a propeller performance curve is generated.

3.1 Mesh Independence

To study mesh dependency the mesh size was globally doubled. The two different meshes were computed for straight ahead conditions with no shaft inclination, allowing for a steady solution. Another possible factor for mesh independence is the distance from the propeller to the inlet and/or outlet. However, as previously stated, prior studies have shown distances as close as $0.72*D$ to be an adequate distance [2] while the current simulations are using a distance of $2*D$. Also, the mesh dependency study was completed on the single blade passage only mesh to save solution time. Because both the single blade passage and the full propeller mesh rely on the same topology it is assumed that the mesh independence results apply for both cases.

To globally double the mesh size, the element count in each direction was increased by a factor of $2^{1/3}$. When this factor is applied to the x,y,z volume the global mesh size is doubled to create a refined mesh. The wall spacing was kept the same between the original and refined mesh to allow use of the same turbulence model.

A propeller performance curve was generated using uniform inflow conditions for the baseline single blade passage mesh and the refined mesh. This curve is seen in Figure 4.

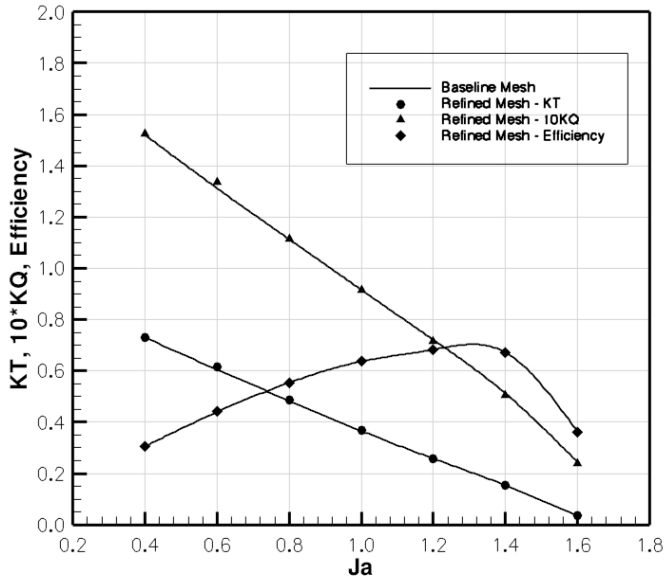

Figure 4 - Mesh dependency study performance curve results

The comparison between the two different mesh sizes gave similar results. The only outlier seems to occur at an advance coefficient of $J_a = 0.6$. This operating condition is very far off design condition as the design advance coefficient is $J_a = 1.2$. Even though this point shows a slight disagreement between the two meshes, the torque seems to be the coefficient with the largest discrepancy, and it varies by less than 2%. It was therefore assumed that the baseline mesh was adequate for the propeller simulations that would follow.

3.2 Experimental Comparisons

Open water experimental data was available for comparison with the numerical results. Open water tests consist of the propeller being driven by a downstream shaft with a fairwater nose cone attached on the upstream surface. This test setup was termed 'open water' because there is no shaft, rudder, or other upstream appendages affecting the inflow to the propeller plane. As previously stated, the numerical simulations were completed with an upstream shaft to more closely replicate actual full scale operating conditions. It was assumed that the effects of the upstream shaft would be minimal on the global force coefficients so that a comparison could still be made without generating a separate domain and mesh for the experimental comparison.

Two sets of experimental data were available for comparison. All tests were conducted at the Naval Surface Warfare Center Carderock Division (NSWCCD). Experiments containing straight flight data sets were conducted in 1986, and a powering experiment was conducted in 1992 which consisted of an inclined shaft arrangement. The shaft inclination angle was 4.8°, which is the angle of inclination that was used for all of the unsteady calculations in this study.

To gain initial confidence in the solution process, the single blade passage simulation was solved for steady flow and compared to the open water experimental data for straight flight from 1986. The simulations were run at a wide range of advance coefficients to compare at off design conditions on both ends of the range. The performance curve comparison is seen in Figure 5.

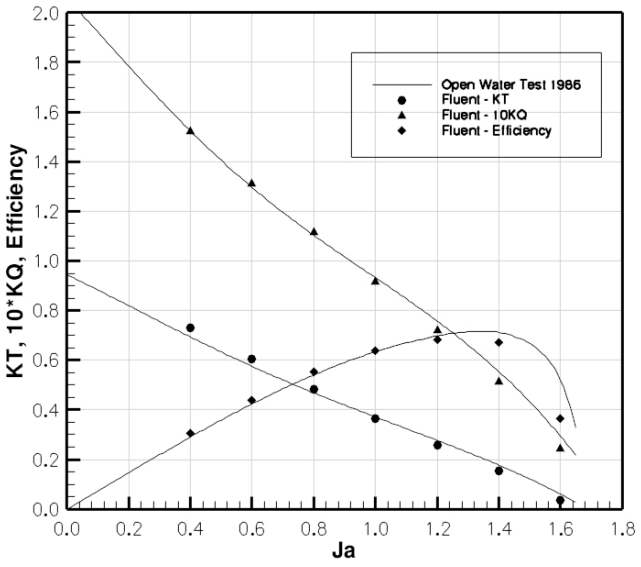

Figure 5 - Propeller performance curve for straight flight

It can be seen in the above figure that good agreement was achieved for the steady condition simulations. The thrust and torque are both slightly over predicted at an advance coefficient less than 1.0 and slightly under predicted at an advance coefficient

above 1.0. The results generally match within 3% except for the efficiency above an advance coefficient of 1.4. These conditions coincide with a higher advance coefficient than design which can produce significant local angles of attack for the blade sections.

To gain confidence in the simulations of the inclined shaft arrangement, which was to be used exclusively for unsteady applications, a performance curve was generated to compare with the inclined shaft experimental data. As previously stated, the shaft inclination angle was set at 4.8° for all of the unsteady simulations. The comparison between the computations and the experiment is seen in Figure 6. It can be seen that the results match generally within 5% of the experimental values. The differences can be attributed to the difference in the test setup as the experimental propeller was driven with a downstream shaft, but further study involving a true open water computation is necessary to further explain the discrepancies.

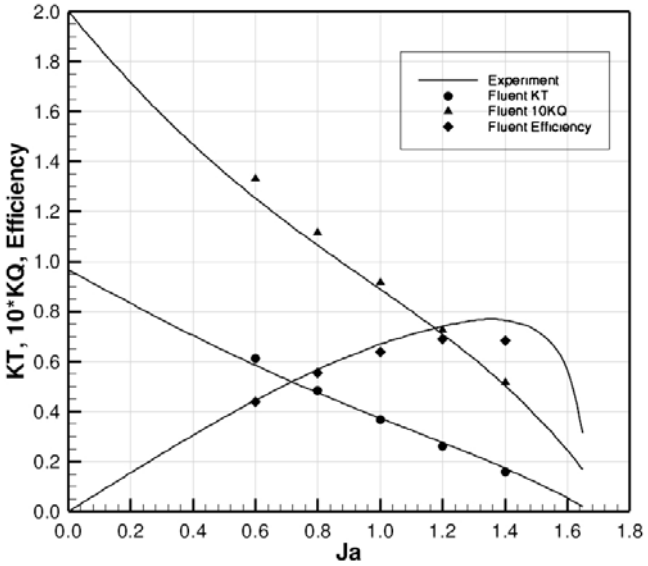

Figure 6 - Propeller performance curve for straight flight with an inclined shaft of 4.8°

3.3 Wake examination

A detailed examination of the flow for an advance coefficient of J_a = 0.98 was completed for the unsteady inclined shaft arrangment. This advance coefficient was chosen because it is just slightly off the design condition of J_a = 1.2. This is the same operating condition that is later used in cross flow calculations to allow for comparisons. A sectional view of tangential velocity countours on the z = 0 plane is shown in Figure 7. This view is of a snapshot at a single time step. It can be noted that the x-direction corresponds to the axial direction, the y-direction to the shaft inclination angle, and the z-direction to any cross flow.

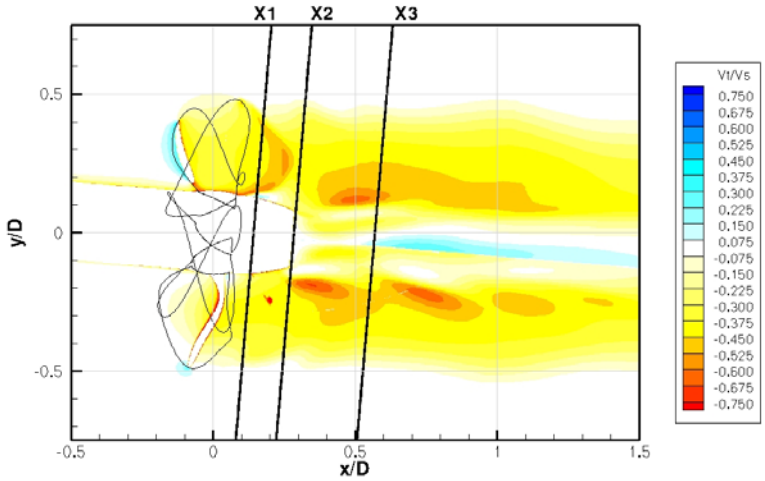

Figure 7 - Contours of tangential velocity on the z=0 plane of an inclined shaft arrangement for $J_a = 0.98$ and no cross flow

The z = 0 plane shown in Figure 7 corresponds to the centerline of the entire domain including the propeller. The x and y axis are normalized by the propeller diameter, and the tangential velocity is normalized by the ship velocity at the chosen operating condition, V_s. Tangential velocity contours are shown to highlight the wake of the propeller. The three plane cuts, X1, X2, and X3, shown in the figure represent y-z planes at different downstream axial locations. These three planes can be used to track the propeller wake as it propagates downstream. Specifically, the X3 plane corresponds to the leading edge of typical rudder placement. Contours of tangential velocity on these three planes can be seen below in Figure 8.

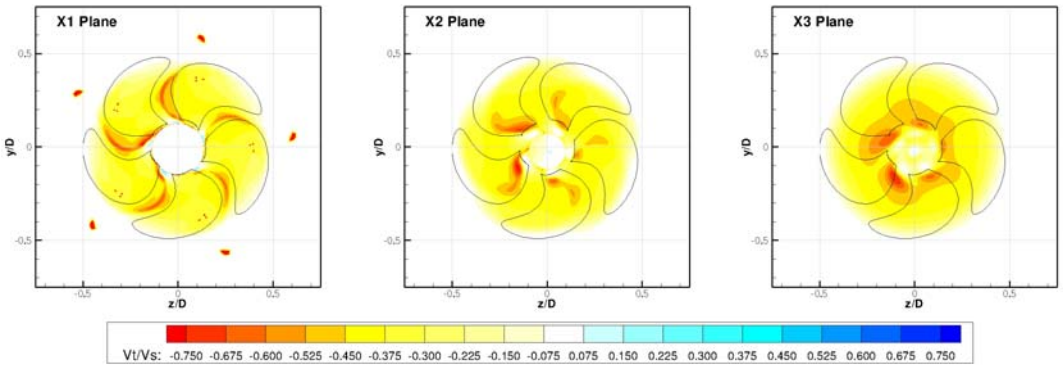

Figure 8 - Contours of tangential velocity on downstream y-z planes

The impact of the propeller on a notional rudder can be seen by examining the transverse cross flow velocities (z-velocity) and the axial velocities. The velocity triangle formed by these two components creates an angle of attack seen locally by a notional rudder. These velocity components are compared on a rake line placed at the leading edge location of a notional rudder. The rake line is located 0.20**D* in the positive transverse direction from the propeller centerline, where *D* is the propeller diameter. The location of this rake line is seen in Figure 9. It can be noted that axially, this line falls on the X3 plane as previously discussed and can be seen in Figure 7.

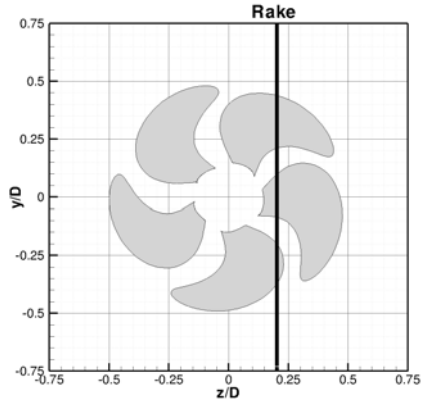

Figure 9 - Illustration of the rake line used for data comparison

The transverse and axial velocities along this rake line can be seen below in Figure 10. Both components of velocity are normalized by the ship speed. It is interesting to note that the velocity profiles are not symmetric due to the influence of the inclined shaft.

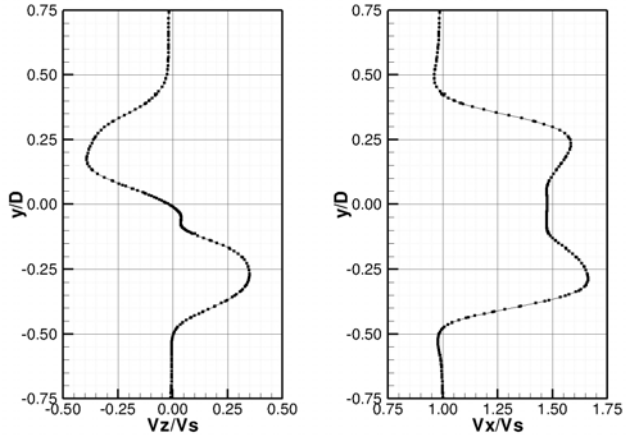

Figure 10 - Transverse and axial velocity along the rake line for a no cross flow case with an inclined shaft

The transverse and axial velocity components can be used to calculate a local angle of attack that is seen by a notional rudder at different radii. A plot of the computed angle of attack along the rake line is seen in Figure 11.

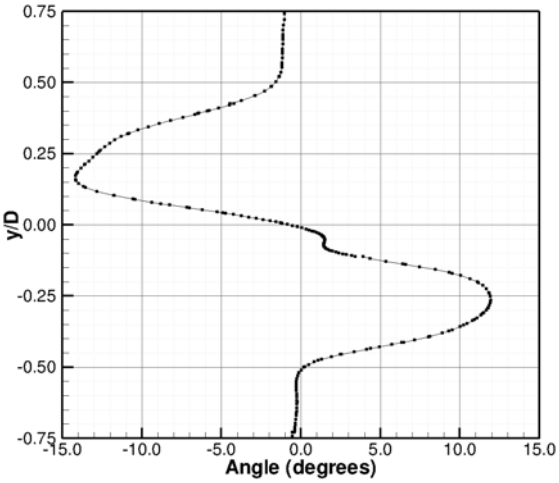

Figure 11 - Local angle of attack seen along the rake line for a no cross flow case with an inclined shaft

3.4 Cross Flow Demonstration

The cross flow cases for this study were simulated using an advance coefficient of 0.98 to allow for a direct comparison with the results previously discussed. Two equal and opposite cross flow angles, +23° and -23°, were run to illustrate the effects of the cross flow direction relative to the propeller rotation. A positive angle of cross flow indicates a positive z-component of velocity. An inclined shaft arrangement was once again utilized to keep the simulation close to actual operating conditions.

A time averaged summary of the forces generated by the propeller in each of the three cases is seen in Table 2. In the table, all of the forces are normalized by the thrust force at 0° cross flow, and all of the moments are normalized by the shaft torque at 0° cross flow. The definition of the x, y, and z directions relative to the propeller and shaft can be seen below the summary in Figure 12.

Force	0°	+23°	-23°
F_X/F_{X0}	1.000	1.066	1.049
F_Y/F_{X0}	-0.059	-0.152	0.012
F_Z/F_{X0}	0.013	-0.275	0.323
M_X/M_{X0}	1.000	1.044	1.026
M_Y/M_{X0}	0.098	0.616	-0.370
M_Z/M_{X0}	-0.097	0.350	-0.598

Table 2 - Time averaged summary of propeller forces using an inclined shaft arrangement

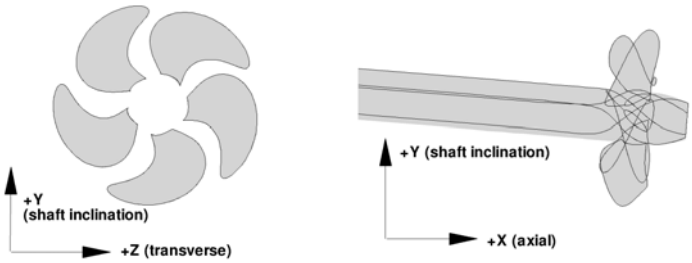

Figure 12 - Illustration of the axis directions relative to the propeller and shaft

It is important to note that the reference thrust force at 0° acts in the negative x-direction and the reference shaft torque at 0° acts about the positive x-axis. The off-axis forces and moments seen in the 0° case are caused by the inclined shaft arrangement previously discussed. It can also be noted that the table shows a significant increase in propeller side forces as a cross flow is introduced. Specifically, a force of approximately +/- 10% of the thrust is introduced in the y-direction and approximately +/- 30% of the thrust in the z-direction. While the force in the z-direction is logical because of the added z-component of velocity due to the cross flow, further examination of pressures on the blade surfaces is required to illustrate the y-component. These surface pressures are illustrated in Figure 13 and Figure 14.

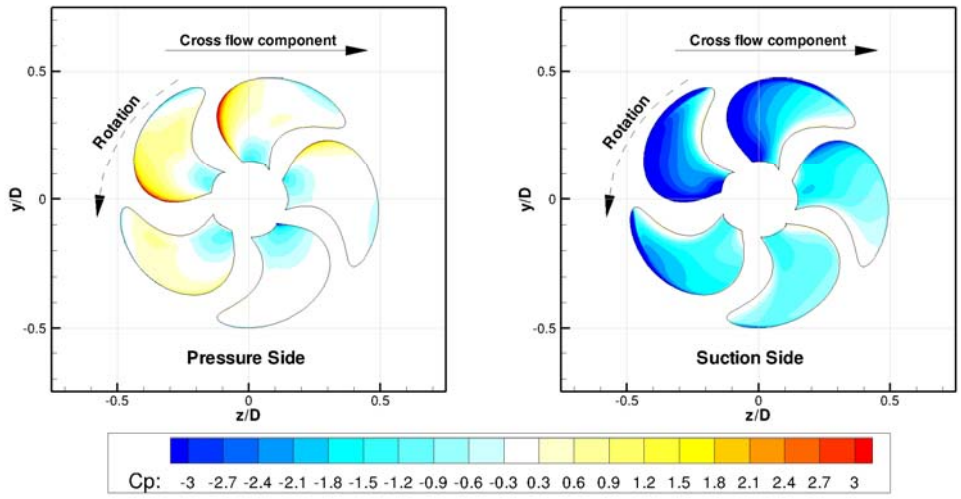

Figure 13 - Blade surface pressure distributions for a cross flow angle of 23°

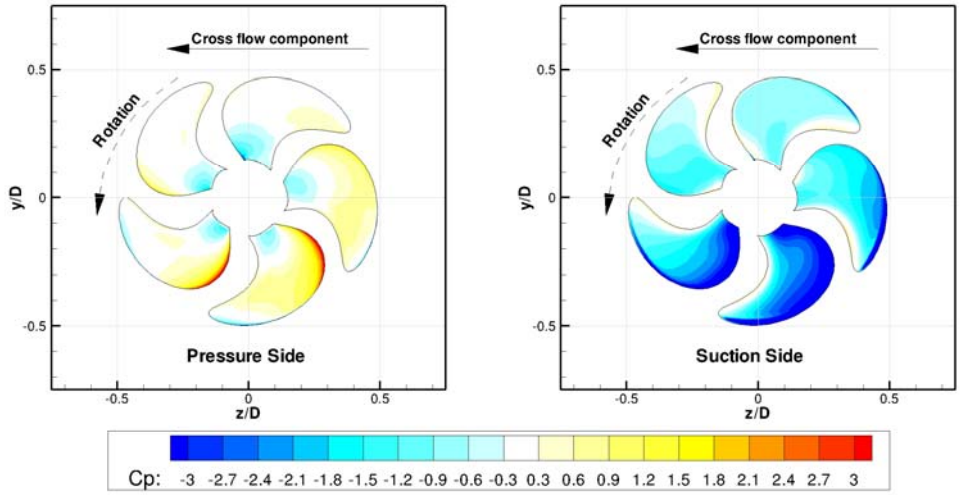

Figure 14 - Blade surface pressure distributions for a cross flow angle of -23°

In the above figures, the coefficient of pressure, C_p, is defined as:

$$C_P = \frac{pressure}{\frac{1}{2}\rho V_S^{\,2}} \tag{6}$$

where V_s is the ship speed, or the total inflow velocity to the domain. It can be seen in the above figures that as the blades rotate into the cross flow component of velocity, a low pressure region is created on the suction side of the blade. This low pressure region causes the difference in y-direction forces that are seen in Table 2. These same low pressure regions explain the strong moments that are seen on the off-rotation axis.

The propeller induced tangential velocities for the cross flow cases can be seen in Figure 15 and Figure 16. It is seen that high tangential velocities are produced on the top and bottom of the propeller where the rotation corresponds to the cross flow component. The positive cross flow corresponds to a z-component that is out of the page, and the propeller is rotating in the clockwise direction (about the negative x-axis).

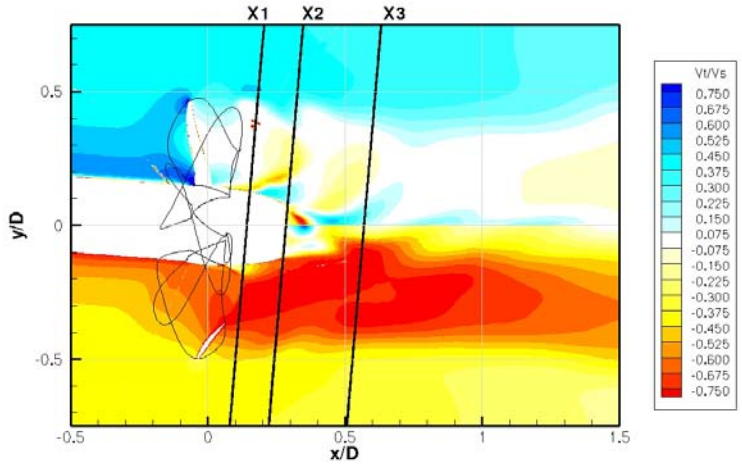

Figure 15 - Tangential velocity contours of a +23° cross flow angle

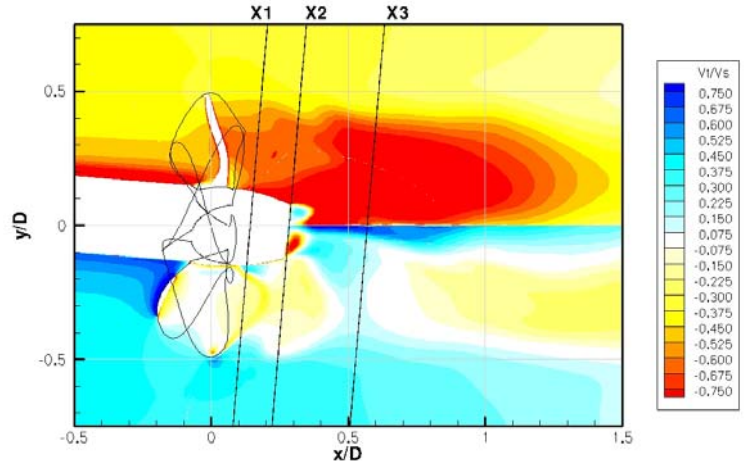

Figure 16 - Tangential velocity contours of a -23° cross flow angle

It can be noted in the above figures that the prescribed cross flow velocity shows up as a tangential velocity during the analysis and is the reason the free stream condition has a tangential component. The same three downstream planes are labeled to give quantitative details of the downstream wake development as well as the influence of the cross flow on its trajectory. These planes are used to show how the induced tangential velocity travels downstream as well as to show the inflow to a notional rudder placed with its leading edge at the X3 plane. To examine the impact of the wake on a rudder, the wake in the X3 plane is examined. Side by side comparisons of the tangential and axial velocities are shown in Figure 17 and Figure 18.

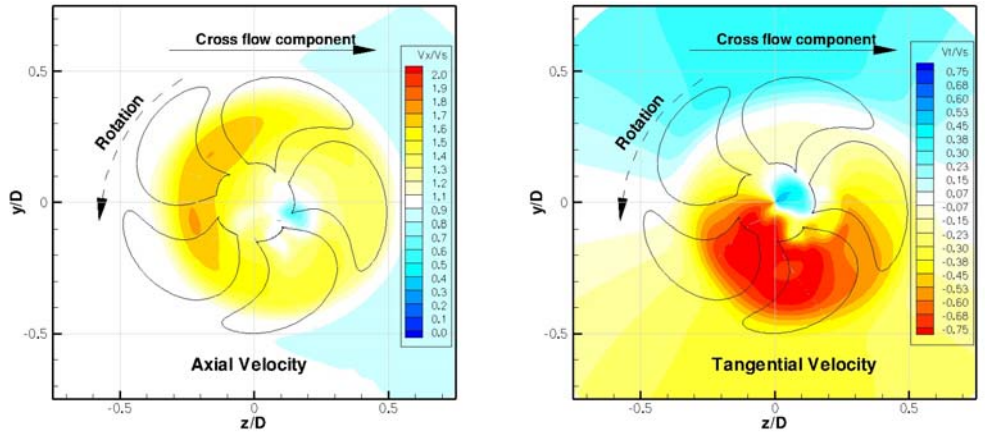

Figure 17 – Axial and Tangential velocity contours at the X3 plane for +23° cross flow

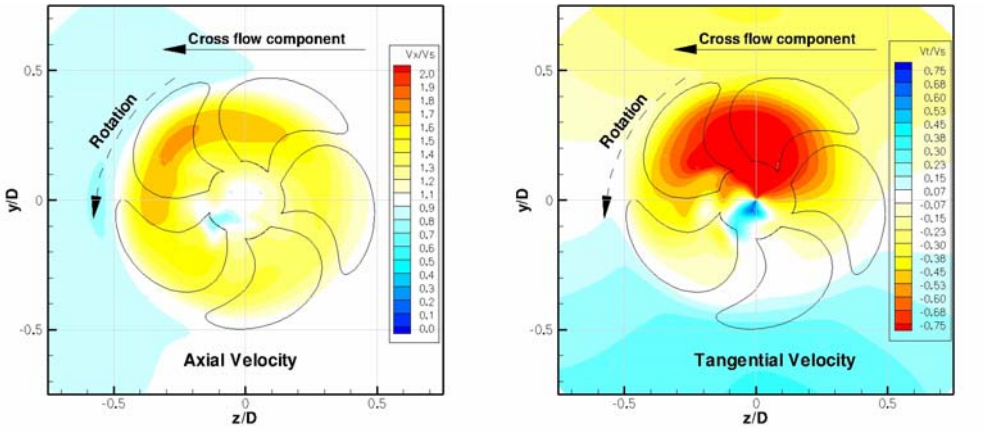

Figure 18 - Axial and Tangential velocity contours at the X3 plane for -23° cross flow

It can be seen that the wake trajectory is slightly off centered due to the cross flow component of velocity. It is also seen that strong local gradients exist and the inflow to any rudder or maneuvering system will be dependent on where it is placed. While the tangential velocity can be detrimental to rudder operations, causing large variations in local angle of attack, the axial velocity jet can be advantageous as it increases the inflow velocity to the rudder giving it a greater ability to create lift. This lift that the rudder creates translates into maneuvering force for the ship system. It can be seen in the above contour plots that a small margin exists where the rudder can be placed to avoid the highest magnitudes of tangential velocity, yet still take advantage of the high axial velocities in the propeller jet. These comparisons can be taken into consideration during the design phase of ship systems but may be outweighed by other practical design considerations.

The effect of the propeller wake on a notional rudder can be quantified by examining the axial and transverse velocities at a rake line that coincides with possible rudder leading edge placement. This rake line is located on the X3 plane and is shifted 0.20**D* in the positive transverse direction as seen previously in Figure 9. This comparison of velocities can be seen for both cross flow angles in Figure 19.

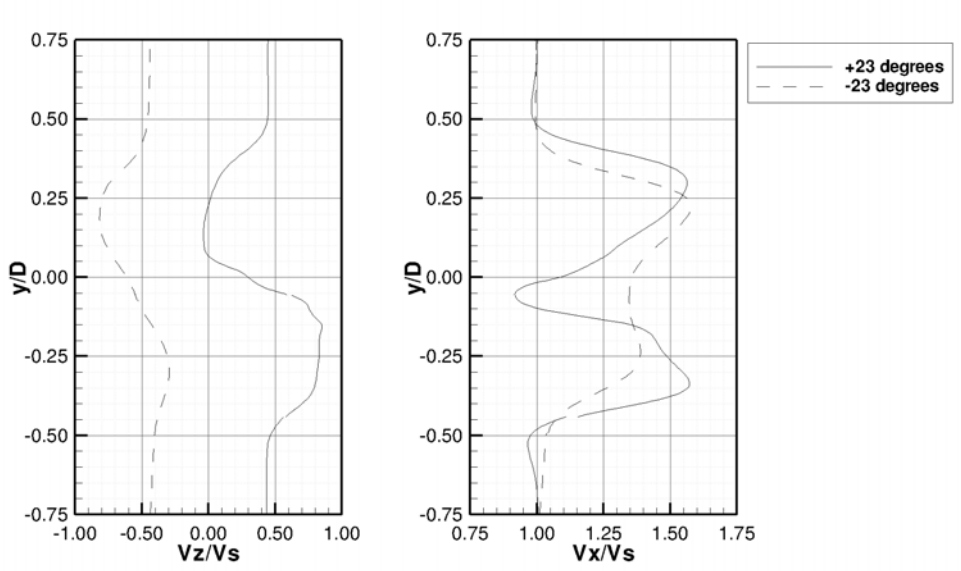

Figure 19 - Transverse and axial velocity comparison along the rake line for both cross flow cases

It can be noted that while the cross flow velocities produce equal and opposite transverse velocity values in the free stream, a unique distribution is given in the propeller wake. This is due to the rotation of the propeller relative to the direction of the cross flow angle.

As a final comparison, the local angle of attack seen at the rake line is plotted for both cross flow angles in Figure 20. It can be noted again that the rotation of the propeller causes unique distributions to be induced by the propeller.

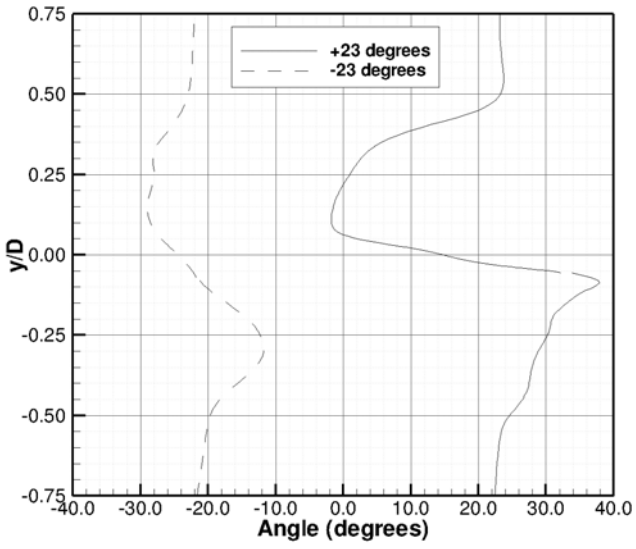

Figure 20 – Comparison of local angle of attack seen along the rake line for both cross flow cases

4 CONCLUSIONS

An unsteady RANS method for simulating a propeller during a ship maneuver has been demonstrated. The method has been supported through mesh independence studies and comparison with experimental data. The proven method was then used to demonstrate a propeller subjected to a cross flow, and a summary of the results with an emphasis on the maneuvering effects was discussed.

The k-ε turbulence model was able to handle the off design conditions which caused flow separation on certain sections of the blades. Future studies could include more extreme cross flow angles that could possibly cause a stall at select blade locations. These studies would require experimental data to be validated using RANS modeling because of the nature of the flows. If a high cross flow angle causes certain sections of the propeller blades to stall, RANS modeling may not be adequate for prediction. It is recommended that if detailed examination of the wake is to be completed, a structured mesh should be used to prevent diffusion in the flow field.

The majority of the results presented are time averaged or circumferentially averaged for system level understanding. The time accurate results shown are only snapshots of instantaneous time steps for demonstrative purposes. However, a detailed time accurate study at any point in the wake is possible using this simulation procedure. Such a study could be used for rudder optimization during the design phase, or for predicting maneuvering characteristics of the propulsor.

Related future work for this simulation method could include a rudder in the domain to measure the forces it produces as it is influenced by the propeller wake. Again, these studies will require experimental data to validate the methods of RANS modeling is to be used. Recent data sets are available for this validation[9]. Extension of the current method to include multiphase modeling could also increase the applicability of the current study[10].

The presented method is adequate as a tool for predicting the propulsor's impact on ship dynamics during operation for a wide range of conditions. The global force results can prove to be useful for larger ship system prediction tools, and the detailed wake examination can be a useful tool in the detailed design and analysis process.

REFERENCES

[1] J.E. Kerwin, T.J. Michael, and S.K. Neely, Improved Algorithms for the Design/Analysis of Multi-Component Complex Propulsors. In proceedings of the *SNAME Propellers/Shafting Symposium* (2006)

[2] S.H. Rhee and S. Joshi, Computational Validation for Flow around a Marine Propeller Using Unstructured Mesh Based Navier-Stokes Solver. *JSME International Journal* **48**, pp562-570 (2005)

[3] C. Dai, R. Miller, S. Percival, Hydrodynamic Effects of Bilge Keels on the Hull Flow During Steady Turns. In proceedings of the *ASME 28th International Conference on Ocean, Offshore, and Arctic Engineering* (2009)

[4] C. Simonsen and F. Stern, RANS Maneuvering Simulation of Esso Osaka with Rudder and a Body-Force Propeller. *Journal of Ship Research*, **Vol. 49, No. 2**, 98-120 (2005)

[5] M. Morgut and E. Nobile, Comparison of Hexa-Structured and Hybrid-Unstructured Meshing Approaches for Numerical Prediction of the Flow Around Marine Propellers, In proceedings of *The First International Symposium on Marine Propulsors* (2009)

[6] B. Chen, F. Stern, Computational Fluid Dynamics of Four-Quadrant Marine-Propulsor Flow. *Journal of Ship Research*, **Vol. 43, No. 4,** 218-228 (1999)

[7] S.E. Kim, S. Schroeder, A Multi-Phase CFD Framework for Predicting Performance of Marine Propulsors. In proceedings of *The Thirteenth International Symposium on Transport Phenomena and Dynamics of Rotating Machinery* (2009)

[8] S.E. Kim, S.H. Rhee, Assessment of Eight Turbulence Models for a Three-Dimensional Boundary Layer Involving Crossflow and Streamwise Vortices. AIAA Paper 2002-0852 (2002)

[9] M. Felli, C. Roberto, and G. Guj, Experimental analysis of the flow field around a propeller-rudder configuration. *Exp Fluids*, **46**, 147-164 (2009)

[10] S. Kinnas, H. Lee, H. Gu, and S. Natarajan, Prediction of Sheet Cavitation on a Rudder Subject to Propeller Flow. *Journal of Ship Research*, **Vol. 51, No. 1**, 65-75 (2007)